



www.sciencemag.org/cgi/content/full/326/5949/112/DC1

Supporting Online Material for

Global Surface Wave Tomography Using Seismic Hum

Kiwamu Nishida,* Jean-Paul Montagner, Hitoshi Kawakatsu

*To whom correspondence should be addressed. E-mail: knishida@eri.u-tokyo.ac.jp

Published 2 October 2009, *Science* **326**, 112 (2009)

DOI: 10.1126/science.1176389

This PDF file includes:

Materials and Methods

Figs. S1 to S4

References

Supporting Online Material (SOM) Global Surface Wave Tomography Using Seismic Hum

Kiwamu Nishida^{1,†} Jean-Paul Montagner,^{1*,2} Hitoshi Kawakatsu¹

¹Earthquake Research Institute, The University of Tokyo,
1-1-1, Yayoi, Bunkyo-ku, Tokyo, Japan

²Institut de Physique du Globe de Paris,
Case 89, 75005 Paris, France

* This work is conducted while the second author was a visiting professor
at the Ocean Hemisphere Research Center of ERI.

†To whom correspondence should be addressed; E-mail: knishida@eri.u-tokyo.ac.jp.

Materials and Method

Data

We analyzed continuous records for 1986–2003 observed at 54 stations of the International Federation of Digital Seismographic Networks (FDSN), which show the lowest ground noise level of vertical components. For each station, the whole record was divided into about 5.6-h segments with an overlap of 1 h. To remove the effects of earthquakes, we discarded all the seismically disturbed segments (S1). Then, cross-correlation functions were calculated between every pair of stations for their common time segments at periods of 100–400 s (Fig. 1A). They show clear global propagations of background Rayleigh waves (5, S2,S3).

We did not use data with a separation distance larger than 160° because of the overlap of R1 and R2 wave packets. The inclusion of R2 data improves the path coverage in the Southern Hemisphere.

Phase-velocity maps

For inversion, we use continuous regionalization (8) with an a priori phase-velocity error of 0.05 km/s and correlation length of 1500 km. Fig. S1 shows phase-velocity maps retrieved by the present method. At shorter periods, the figure shows, as expected, low-velocity anomalies beneath subduction zones and mid-ocean ridges. In the continental regions (primarily beneath shields) it shows high-velocity anomalies. As the period becomes longer, the low-velocity anomalies beneath subduction zones disappear and high-velocity anomalies due to subducted slabs can be observed. The six resulting phase-velocity maps exhibit a dispersion curve at each point.

Strong heterogeneity in the source distribution will cause apparent phase-delay anomalies. The source distribution of seismic hum, as estimated from the observed cross-correlation functions, shows a dominant long-wavelength structure (angular degree < 4) (5). In such a case, phase-delay measurements with synthetic cross-correlation functions for heterogeneous sources would not be very different from those with homogeneous sources (5). Therefore, we attribute the observed discrepancy to the effect of the lateral heterogeneity of the Earth and neglect the effects of source heterogeneity.

Crustal correction

Heterogeneous distributions of shallow layers (topography, ocean bathymetry, sediment layers and crustal thickness) affect phase-velocity anomalies even at long periods. It is important to assess their effects to remove bias in the deep anomalies due to the shallow structure. Crustal

corrections are calculated as follows. A local 1-D model is constructed for each $2^\circ \times 2^\circ$ grid. We construct the model by merging a crustal model (crust2.0) (S4) with a global 1-D model (PREM) (7). The crustal model has a maximum of seven layers: water, ice, soft sediment, hard sediment, upper crust, middle crust and lower crust. Then we calculated the phase velocity $C(f)$ of the local 1-D models at frequency f . Crustal corrections to the phase-velocity anomaly, $(C(f) - C_0(f))/C_0(f)$, are evaluated at frequency f . Here $C_0(f)$ is the dispersion curve for PREM. To correct our model, we resample the correction ($2^\circ \times 2^\circ$ grid) into a $5^\circ \times 5^\circ$ -grid model. The procedure for crustal correction at a period of 120 s is shown in Fig. S2. This figure shows significant correction at a period of 120 s. The corrections reduce low-velocity anomalies caused by strong crustal heterogeneities, in particular, at the Himalayas and Andes.

Comparison with other global models

Our model compares well with other three global tomographic models created using earthquakes (Fig. S3): (i) Harvard model (S5), (ii) Scripps model (S6) and (iii) Berkeley model (S7). We calculated the correlation coefficients of our model with each of the three models (Fig. S3 right). At shallow depths (above 300 km), the correlation coefficients are about 0.7, indicating high consistency between models. Notably, a good agreement is obtained in the depth range 100–500 km, which corresponds to the maximum depth sensitivity of Rayleigh waves at periods of 100–400 s. As the deeper parts of the other models are also constrained by long-period body waves and overtones of surface waves the difference in data type reduces the cross-correlation coefficients with depth below 500 km. Our model, created without referring to earthquakes and though of limited resolution, displays robust features that are in good agreement with those of conventional tomographic models derived from earthquake data.

Synthetic test of cross-correlation analysis on Mars

Our tomographic approach has potential applications in planetary exploration, particularly in investigating the deep internal structures of the planet Mars. As the existence of marsquakes is questionable, the applicability of conventional earthquake tomography is not guaranteed. However, Martian atmospheric disturbances might excite background long-period Rayleigh waves on this planet (2,S8,S9,S10), which might then be used to retrieve Green's-function-like signals between stations of future Martian seismic networks.

To evaluate the feasibility of our technique on Mars, we developed synthetic cross-correlation functions with the assumption that random dynamic pressure disturbances on the Martian surface excite background Rayleigh waves. We make the following three assumptions regarding the random pressure sources: (i) The power spectra of surface pressure are 1% of those of the Earth (S10) ($10 \text{ Pa}^2/\text{Hz}$ at 1 mHz with f^2 dependency, where f is frequency). This is based on measurements of surface Martian atmospheric pressure in the Mars Pathfinder mission (S11). (ii) The correlation length is five times larger (5 km at period of 100 s) than that of the Earth (2, S10). And (iii) we calculated synthetic cross-correlation functions with an assumption of the theoretical 1-D internal structure of Mars (S12). Dust storms and dust devils are expected to be stronger excitation sources but are not considered here for simplicity. We also assume that seismometers are installed at five sites –the landing sites of the Viking 1 and Viking 2 landers, Mars Pathfinder Rover and Mars Exploration Rovers Spirit and Opportunity (S13)– for an observation time period of about a half year. The local noise level at the sites is assumed to be similar to that at quiet sites on the Earth. The resulting cross-correlation functions (Fig. S4) show clear R1 and R2 wave packets, thus proving the feasibility of our method on Mars. For a seismic network of five stations (20 minor and major arc paths), it should be possible to retrieve 3-D S-wave velocity structures up to harmonic degree 4. Thus, seismic observation of the hum

and ambient noise induced by coupling between the atmosphere and solid ground is potentially an exploration tool for understanding of the dynamic status of the planet Mars as well as other terrestrial planets with an atmosphere and/or oceans.

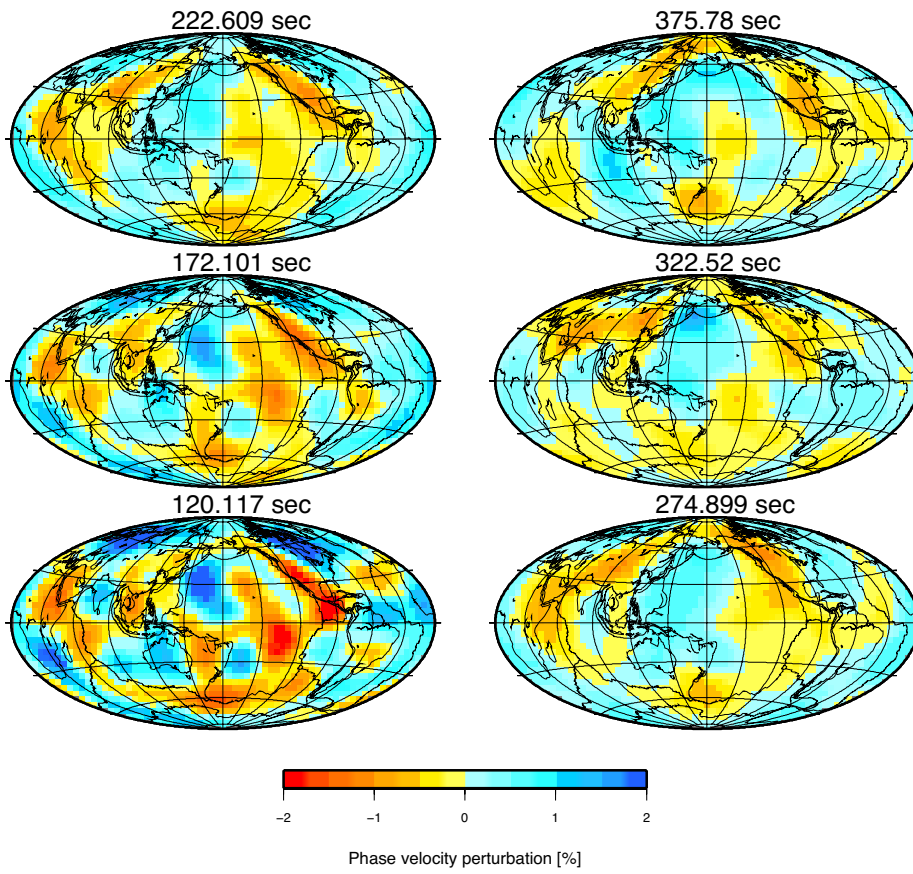


Fig. S1.

Phase-velocity maps in the period range 120–376 s.

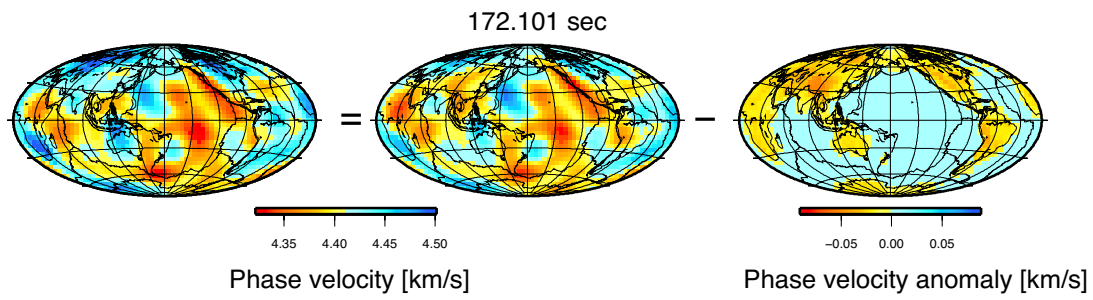


Fig. S2.

Phase-velocity map with crustal correction at a period of 172 s (left). The crustal correction (right) and observed original phase-velocity maps (centre) are also displayed.

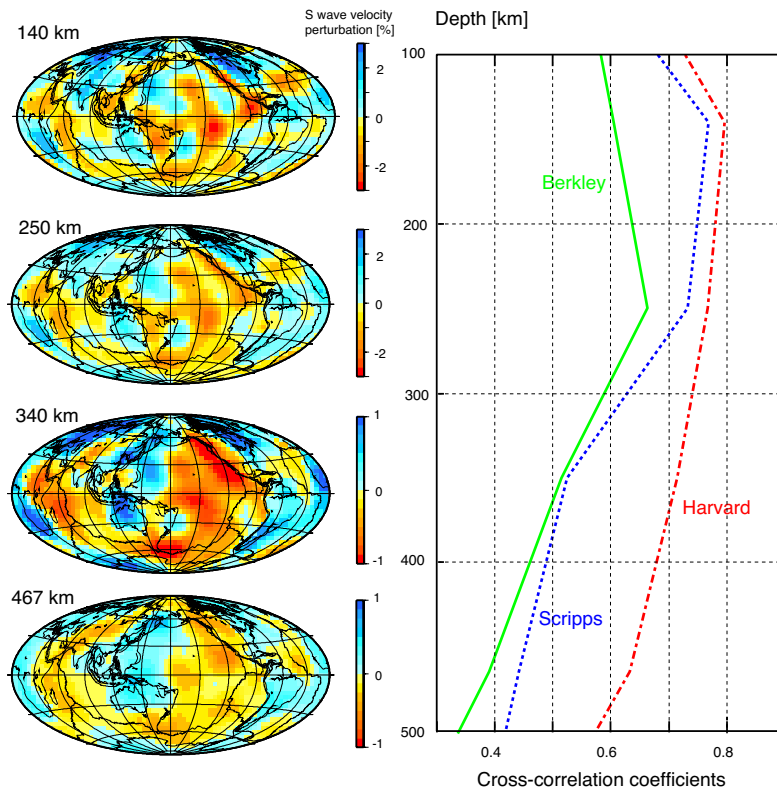


Fig. S3.

Left: S-wave velocity structure at depths from 140 to 467 km. Right: Cross-model correlation coefficients between our model and three other models (Harvard model (S5), Scripps (S6) and Berkeley (S7)) as a function of depth. Models are sampled at $5^\circ \times 5^\circ$ grid points for comparison.

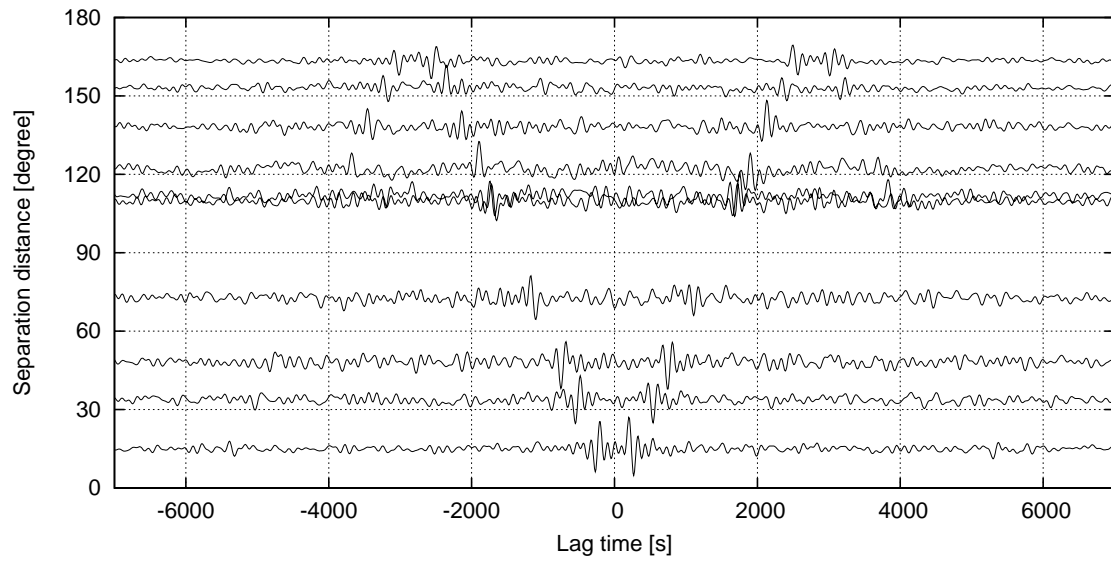


Fig. S4.

Example of cross-correlation functions of synthetic Mars hum records between pairs of stations from 2 to 10 mHz.

Supporting references

- S1 K. Nishida, N. Kobayashi *J. Geophys. Res.* **104**, 28,741, (1999).
- S2 G. Ekström, *J. Geophys. Res.* **106**, 26,483 (2001).
- S3 K. Nishida, N. Kobayashi, Y. Fukao, *Geophys. Res. Lett.* **29**, 1413 (2001).
- S4 C. Bassin, G. Laske, G. Masters, *EOS Trans AGU* **81**, F897 (2000).
- S5 Y. J. Gu, A. M. Dziewonski, W. J. Su, G Ekström, *J. Geophys. Res.* **106**, 11169 (2001).
- S6 G. Masters, G. Laske, H. Bolton, A. Dziewonski, *The Relative Behaviour of Shear Velocity, Bulk Sound Speed, and Compressional Velocity in the Mantle: Implications for Chemical and Thermal Structure* (AGU, Washington, 2000).
- S7 C. Mégnin, B. Romanowicz, *Geophys. J. Int.* **143**, 709 (2000).
- S8 P. Lognonné, *Annu. Rev. Earth Planets. Sci.* **33**, 571 (2005).
- S9 P. Lognonné, C. L. Johnson, *Planetary Seismology* (Elsevier, Amsterdam, 2007), pp. 69–122.
- S10 N. Suda, C. Mitani, N. Kobayashi, K. Nishida, *Eos Trans. AGU* **83**, 47 (2002).
- S11 Schofield, J. T. et. al, *Science* **278**, 1752 (1997).
- S12 E. Okal, D. L. Anderson, *ICARUS* **33**, 514 (1978).
- S13 M. H. Carr, *The Surface of Mars, Cambridge Planetary Science Series No. 6* (Cambridge University Press, Cambridge, 2007).